

# A 25-year data record of atmospheric ozone in the Pacific from Total Ozone Mapping Spectrometer (TOMS) cloud slicing: Implications for ozone trends in the stratosphere and troposphere

J. R. Ziemke<sup>1</sup> and S. Chandra<sup>1</sup>

Goddard Earth Sciences and Technology Center, Baltimore, Maryland, USA

P. K. Bhartia

NASA Goddard Space Flight Center, Greenbelt, Maryland, USA

Received 10 December 2004; revised 3 May 2005; accepted 31 May 2005; published 13 August 2005.

[1] The newly reprocessed solar backscatter ultraviolet (SBUV) and Total Ozone Mapping Spectrometer (TOMS) version 8 data from 1979 to 2003 are used to estimate the seasonal cycle, latitude dependence, and long-term trends in ozone averaged over the Pacific region (120°W to 120°E) in three broad layers of the atmosphere: upper stratosphere (32 hPa and above), lower stratosphere (32 hPa to tropopause), and the troposphere. The ozone amount in these layers is derived by first determining stratospheric column ozone in the Pacific from TOMS using deep convective clouds, which are numerous in the region. Tropospheric column ozone (TCO) for the Pacific is then determined by taking the difference between total column ozone and stratospheric column ozone. This “cloud-slicing” technique is extensively tested from the tropics extending to ±60° latitude using stratospheric ozone data from the Stratospheric Aerosol and Gas Experiment II instrument. The validity of the cloud-slicing technique in obtaining TCO is also tested using data from ozonesondes over a wide range of latitude. SBUV ozone profiles are used to measure upper stratospheric column ozone for the Pacific region. Lower stratospheric column ozone is then derived from the difference between stratospheric column ozone and upper stratospheric column ozone. This process yields a unique 25-year record of Pacific mean ozone in three atmospheric layers covering all latitudes and seasons. The analysis of the data shows that the seasonal cycles, latitude dependence, and trends in these layers are substantially different. Over the 25-year record most ozone depletion has occurred in the lower stratosphere below ~25 km altitude. In middle and high latitudes, ozone losses are 3–4 times larger in the lower stratosphere compared with the upper stratosphere, even though the ozone amounts in the two regions are about the same. For the troposphere, TCO shows a statistically significant upward trend in the midlatitudes of both hemispheres but not in the tropics.

**Citation:** Ziemke, J. R., S. Chandra, and P. K. Bhartia (2005), A 25-year data record of atmospheric ozone in the Pacific from Total Ozone Mapping Spectrometer (TOMS) cloud slicing: Implications for ozone trends in the stratosphere and troposphere, *J. Geophys. Res.*, 110, D15105, doi:10.1029/2004JD005687.

## 1. Introduction

[2] In recent years the convective cloud differential (CCD) method has been used extensively to derive stratospheric column ozone (SCO) and tropospheric column ozone (TCO) in the tropics using Total Ozone Mapping Spectrometer (TOMS) version 7 data [e.g., Ziemke *et al.*, 1998; Chandra *et al.*, 2002]. These data, together with similar data derived from combined TOMS and Upper

Atmosphere Research Satellite (UARS) Microwave Limb Sounder measurements, have been used to characterize variabilities in SCO and TCO from monthly to long-term trends, including (1) intraseasonal, interannual, and decadal changes associated with the Madden-Julian Oscillation, quasi-biennial oscillation (QBO), El Niño, La Niña, and solar cycle [Chandra *et al.*, 1998, 1999; Ziemke and Chandra, 1999, 2003a, 2003b], and (2) the relative influence of dynamics and chemistry on TCO in the tropical region with special reference to the 1997 El Niño [Chandra *et al.*, 2002, 2003]. The CCD method is a special case of the general cloud-slicing method [Ziemke *et al.*, 2001, 2003; Ahn *et al.*, 2003] and takes advantage of the fact that UV-measuring instruments, such as TOMS, cannot measure ozone lying below dense water vapor clouds. The key

<sup>1</sup>Also at NASA Goddard Space Flight Center, Greenbelt, Maryland, USA.

element in determining ozone information from the cloud slicing method is to have simultaneous and collocated measurements of both above-cloud-column ozone and cloud top pressure. In contrast, the CCD method assumes that one can make an accurate estimate of SCO using high reflecting convective clouds (reflectivity  $R > 0.9$ ) that reach at or near the tropopause level in the tropical Pacific region. The CCD method further assumes that SCO is zonally invariant within the latitude range  $15^{\circ}\text{N}$  to  $15^{\circ}\text{S}$ . With these assumptions, TCO in tropical latitudes can be calculated at any location by differencing low-reflectivity ( $R < 0.2$ ) gridded total column ozone and high-reflectivity ( $R > 0.9$ ) SCO from the Pacific region. In general, high reflecting clouds do not often reach tropopause height, and the column ozone above the cloud may vary considerably even when  $R > 0.9$ . As a practical solution, SCO is calculated using only the smallest values of above-cloud-column ozone in each  $5^{\circ} \times 5^{\circ}$  bin. These minimum values are then averaged over the longitude band  $120^{\circ}\text{W}$  to  $120^{\circ}\text{E}$ , which encompasses the eastern and western Pacific.

[3] Our study of the CCD method shows that the determination of SCO and TCO from high reflecting convective clouds is not limited to tropical latitudes. Such clouds exist at all latitudes, particularly in the Pacific region. This allows the determination of both SCO and TCO at middle and high latitudes in both hemispheres over the Pacific, which is consistent with similar measurements from Stratospheric Aerosol and Gas Experiment II (SAGE II) [Wang *et al.*, 2002, and references therein]. When combined with solar backscatter ultraviolet (SBUV) measurements, which determine upper stratospheric column ozone (USCO) for 0–32 hPa, the CCD method yields ozone measurements in three broad layers of the atmosphere averaged over the Pacific, extending from the tropics to middle and high latitudes: upper stratosphere (32 hPa and above), lower stratosphere (32 hPa to tropopause), and the troposphere.

[4] The purpose of this study is to establish viable long-record reference benchmark data sets of stratospheric and tropospheric ozone in the Pacific region from combined TOMS cloud-slicing and SBUV measurements using recently reprocessed data based on the version 8 algorithm (see Ozone Monitoring Instrument (OMI) Algorithm Theoretical Basis Document (ATBD) Web page <http://www.knmi.nl/omi/research/documents/index.html>). These data, which cover a 25-year period from 1979 to 2003, are used to characterize seasonal cycles and trends in (1) total column ozone, (2) SCO (above tropopause), (3) USCO (above 32 hPa), (4) lower stratosphere column ozone (LSCO) (32 hPa to tropopause), and (5) TCO. This paper is arranged as follows: Section 2 describes satellite ozone measurements. Section 3 describes TOMS and SAGE II SCO comparisons in the tropics. Section 4 describes the extension of TOMS SCO measurements to extratropical latitudes. Section 5 offers TOMS/ozonesonde TCO comparisons. Section 6 explains seasonal variation of ozone in the different regions of the atmosphere. Section 7 explains ozone trends, and section 8 provides a summary.

## 2. Ozone Measurements

[5] The CCD data used in this study are from TOMS version 8 level 2 processing. Details regarding the TOMS

version 8 processing may be obtained from the OMI ATBD. Version 8 includes many modifications from version 7, including improved a priori tropospheric ozone, an aerosol and sea glint correction, in situ tropospheric efficiency correction, and an Earth Probe (EP) offset adjustment of around  $-5$  Dobson units (DU) ( $1 \text{ DU} = 2.69 \times 10^{20} \text{ molecules m}^{-2}$ ) to  $-7$  DU (largest adjustment outside the tropics). TOMS TCO and SCO measurements in our investigation were gridded to  $5^{\circ} \times 5^{\circ}$  bins covering all longitudes in the low-latitude tropics and the Pacific region ( $120^{\circ}\text{W}$  to  $120^{\circ}\text{E}$ ) lying within latitudes  $60^{\circ}\text{S}$  to  $60^{\circ}\text{N}$ . Temporal coverage is monthly and spans January 1979 to April 1993 (Nimbus 7 TOMS) and August 1996 to August 2003 (Earth Probe TOMS). All total column ozone from TOMS was derived from essentially clear-sky footprint scenes with reflectivity  $R < 0.2$ .

[6] USCO, representing the pressure band from 0 to 32 hPa ( $\sim 25$  km altitude), was determined from SBUV version 8 ozone profiles for 1979–2003. Selected SBUV measurements from Nimbus 7 (1979–1988), National Oceanic and Atmospheric Administration (NOAA) 11 (1989–1995), and NOAA 16 (1996–2003) satellites were combined to form a 25-year continuous data set. Column ozone in the 0- to 32-hPa pressure range represents precise measurements from SBUV. (Difficulties arise for ozone measurements lying below the ozone number density peak, which varies with latitude but is generally below 32 hPa in altitude.) The purpose of including SBUV column ozone is to derive upper and lower stratospheric column ozone by differencing with CCD SCO.

[7] Version 8 succeeds version 6 for the SBUV algorithm (there was no version 7 released for SBUV data). Among several improvements from version 6, version 8 includes (1) reduced sensitivity to atmospheric temperature, aerosols, clouds, and surface reflectivity; (2) improved a priori ozone profile climatology, including tropospheric climatology; (3) improved modeling of multiple scattering and clouds; (4) improved terrain height; and (5) reduced use of longer wavelengths to derive ozone profile information (thus reducing scattering effects affecting the longer wavelengths). The SBUV version 8 profile algorithm is discussed briefly by Bhartia *et al.* [2004] and on the merged ozone Web site ([http://hyperion.gsfc.nasa.gov/Data\\_services/merged](http://hyperion.gsfc.nasa.gov/Data_services/merged)).

[8] It is generally recognized that SAGE stratospheric ozone data have become a standard long-record reference field for comparison with other stratospheric ozone measurements. We have incorporated SAGE II version 6.2 measurements of SCO to compare with TOMS CCD and SBUV stratospheric ozone. SAGE II version 6.2 ozone measurements show generally small changes from version 6.1 (which is described by Wang *et al.* [2002]). Ozone data from SAGE were gridded to daily  $5^{\circ} \times 5^{\circ}$  bins and then averaged as monthly ensembles. The SAGE data were obtained from the NASA Distributed Active Archive Center. Ozone profiles for SAGE version 6.2 have several advantages over version 6.1, including an improved aerosol correction and an oxygen dimer ( $\text{O}_2\text{-O}_2$ ) correction at 525-nm and 1020-nm channels (a brief discussion of the data may be obtained at [http://www-sage2.larc.nasa.gov/data/v6\\_data/](http://www-sage2.larc.nasa.gov/data/v6_data/)). The SAGE measurements in our study extend from October 1984 through September 2003, with

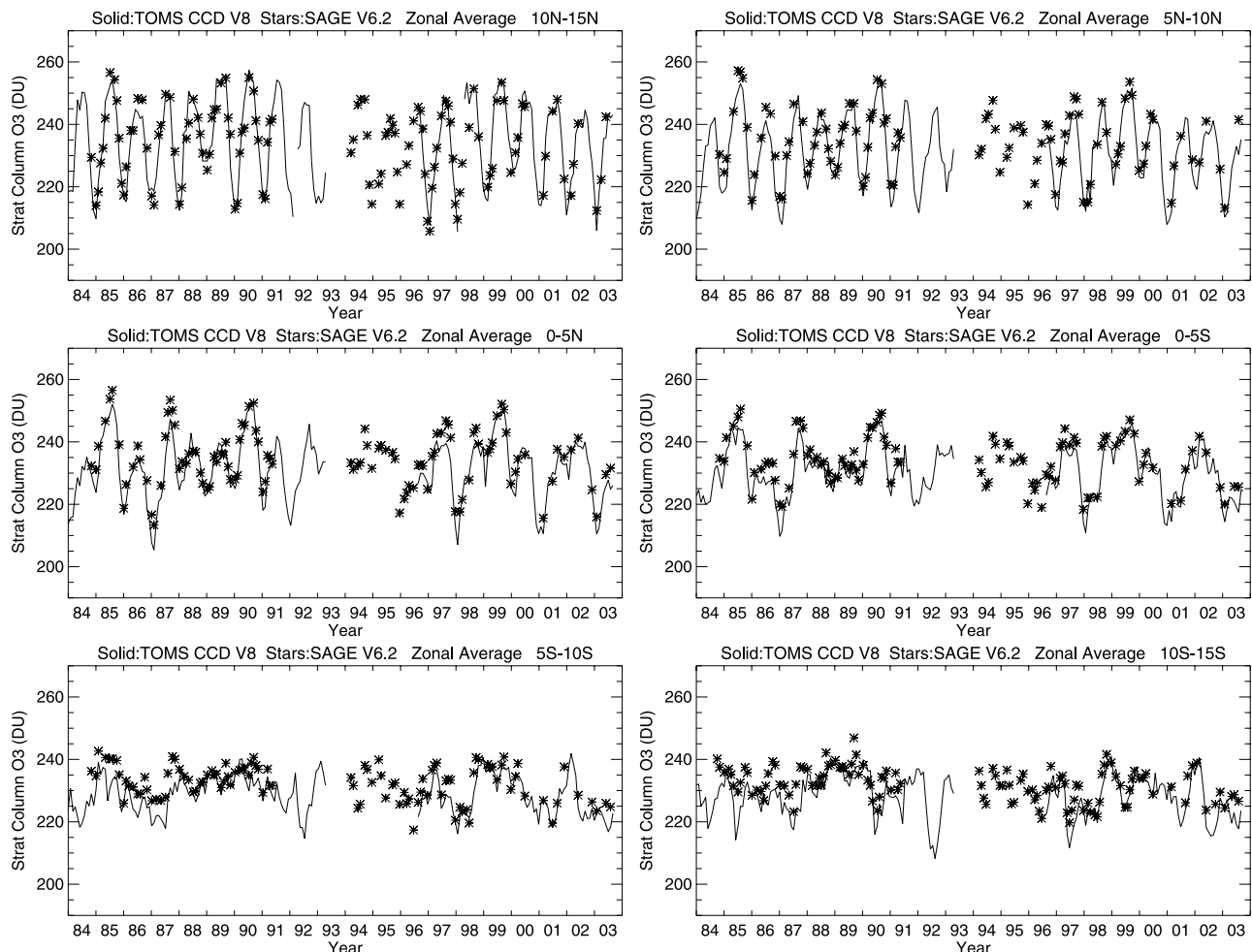


**Figure 1.** Comparisons of monthly stratospheric column ozone (SCO) in Dobson units (DU) from Total Ozone Mapping Spectrometer (TOMS) convective cloud differential (CCD) (solid lines) and Stratospheric Aerosol and Gas Experiment II (SAGE II) (stars) for six  $5^\circ$  latitude bands (indicated) extending from  $15^\circ\text{S}$  to  $15^\circ\text{N}$  in the (top) Northern Hemisphere, (middle) equatorial latitudes, and (bottom) Southern Hemisphere. The CCD measurements are Pacific averages ( $120^\circ\text{W}$ – $120^\circ\text{E}$ ). SAGE II SCO was determined by including all measurements available along longitude for calculating a zonal mean.

June 1991 through 1993 flagged as missing because of effects from the Mount Pinatubo volcanic aerosols. SCO from SAGE ozone profiles entails column integration of ozone mixing ratio in pressure from the top of the atmosphere down to the tropopause, which was deduced from National Centers for Environmental Prediction analyses using a  $2\text{ K km}^{-1}$  lapse rate criterion.

### 3. TOMS and SAGE SCO Time Series Comparisons in the Tropics

[9] Figure 1 compares monthly SCO from TOMS CCD (solid curves) and SAGE (stars) for six  $5^\circ$  latitude bands extending from  $15^\circ\text{S}$  to  $15^\circ\text{N}$  (indicated). “Zonal average” in Figure 1 refers to zonal averaging over the Pacific for CCD, and for SAGE it means at least 10 profile measurements per month in a given  $5^\circ$  latitude band (neither measurement is a true “zonal mean”).

[10] As seen in Figure 1, both the magnitude and temporal characteristics of TCO derived from CCD and

SAGE are in excellent agreement even though the two measurements are not intercalibrated. SCO from both TOMS CCD and SAGE exhibits a dominant annual cycle in northern latitudes. TOMS CCD and SAGE also show similar interannual variations ( $\sim 10$ - to  $15$ -DU changes) over the 20-year record shown. In equatorial latitudes  $5^\circ\text{S}$ – $5^\circ\text{N}$  (two middle plots), variability in SCO is primarily a coupling of annual cycle with the QBO. In southern latitudes  $5^\circ\text{S}$ – $15^\circ\text{S}$  (two bottom plots), variability in SCO resembles a weak annual cycle coupled with some amount of interannual QBO-related changes in the  $10^\circ\text{S}$ – $15^\circ\text{S}$  band and a stronger QBO signal in the  $5^\circ\text{S}$ – $10^\circ\text{S}$  latitude band. An important characteristic in Figure 1 is the large reduction in the SCO annual cycle going from northern to southern latitudes. This feature in SCO was described in an earlier study by Ziemke and Chandra [1999] using TOMS version 7 CCD measurements. We note that preliminary analysis of Goddard three-dimensional Global Modeling Initiative SCO (A. Douglass and R. S. Stolarski, personal communication, 2004) over a



**Table 1a.** Statistical Measurements of TOMS SCO Minus SAGE SCO for the Time Series Plotted in Figures 1 and 3<sup>a</sup>

Latitude	<i>N</i>	Diff, DU	RMS, DU	<i>r</i>
55°N–60°N	89	5.2	22.6	0.90
50°N–55°N	114	–3.5	22.0	0.84
45°N–50°N	136	–7.9	23.8	0.79
40°N–45°N	130	–12.7	21.9	0.83
35°N–40°N	129	–13.4	19.3	0.81
30°N–35°N	127	–9.5	13.3	0.84
25°N–30°N	125	–3.0	8.2	0.90
20°N–25°N	121	–0.3	7.8	0.89
15°N–20°N	106	1.3	7.7	0.87
10°N–15°N	93	–0.6	4.7	0.94
5°N–10°N	87	–3.3	4.9	0.95
0°–5°N	91	–2.9	4.4	0.94
0°–5°S	87	–2.9	4.0	0.95
5°S–10°S	90	–3.4	4.6	0.85
10°S–15°S	102	–3.7	5.4	0.78
15°S–20°S	113	–1.7	5.6	0.77
20°S–25°S	119	2.1	6.2	0.85
25°S–30°S	125	4.3	7.5	0.92
30°S–35°S	128	4.2	9.0	0.93
35°S–40°S	127	2.7	11.7	0.93
40°S–45°S	127	1.7	15.9	0.89
45°S–50°S	123	1.0	19.8	0.83
50°S–55°S	85	6.3	26.9	0.78
55°S–60°S	74	8.7	28.1	0.70

<sup>a</sup>Definitions are TOMS, Total Ozone Mapping Spectrometer; SCO, Stratospheric Column Ozone; SAGE, Stratospheric Aerosol and Gas Experiment; *N*, number of collated measurements in each latitude band; Diff, TOMS SCO minus SAGE SCO mean difference; RMS, calculated root-mean-square of the difference time series; *r*, calculated correlation between the two time series; and DU, Dobson units (1 DU =  $2.69 \times 10^{20}$  molecules m<sup>–2</sup>).

corresponding long time record shows similar hemispheric differences in annual cycles in tropical latitudes.

[11] Statistical comparisons of the two time series are given in Table 1a, which lists their relative bias, RMS difference, and correlation statistic (*r*). Table 1a also lists the number of data points (*N*) used in calculating the statistical parameters. We note that Table 1a also shows comparisons between TOMS and SAGE SCO for latitudes beyond  $\pm 15^\circ$  (discussed in section 4). On average, TOMS SCO in the tropics between  $15^\circ\text{S}$  and  $15^\circ\text{N}$  is  $\sim 2.8$  DU less than SAGE SCO. For the  $10^\circ\text{N}$ – $15^\circ\text{N}$  latitude band their difference is less than 1 DU. RMS differences for the latitude band  $15^\circ\text{S}$ – $15^\circ\text{N}$  average around 4–5 DU. Correlation values between TOMS and SAGE SCO are largest ( $>0.9$ ) in the Northern Hemisphere (NH), because of a dominant annual cycle with peak values around August.

#### 4. Extension of TOMS SCO Measurements to Extratropical Latitudes

[12] As discussed in section 1, high convective clouds reaching tropopause height are essential to the efficacy of CCD SCO and TCO measurements. Results from this study indicate that this condition is not limited to tropical latitudes but persists well outside the tropics to middle and high latitudes in both hemispheres in the Pacific region. Unfortunately, it is not possible to determine the cloud top pressure with current TOMS measurements. Therefore the assumption that some of the high reflecting clouds reach the tropopause height can be verified only indirectly, i.e., by comparing the CCD-derived SCO with SAGE SCO for tropical latitudes, as in section 3. However, the assumption

of zonal invariance in SCO is not valid outside the tropics, particularly in winter and spring months. The applicability of the CCD method outside the tropics is therefore limited to the Pacific region.

[13] Figure 2 compares zonal variability of SCO in the low-latitude tropics (top plot) and NH subtropics (bottom plot) using SAGE II data from 1984 to 2003. SCO is averaged over the Atlantic and Pacific regions and the difference (Atlantic minus Pacific) reflects the zonal variability present. It is noted that since SAGE is an occultation experiment, monthly SCO zonal differences plotted in Figure 2 are derived from only 1 or 2 days of SAGE measurements. These differences may therefore be influenced by episodic tropical waves in the stratosphere, such as Kelvin waves, mixed Rossby-gravity waves, normal modes, and equatorial Rossby waves. All of these dynamical waves may produce planetary-scale and smaller-scale zonal variation  $\sim 3$ – $5$  DU in SCO (peak to peak) with periods from several days to around 1–2 weeks [Ziemke and Stanford, 1994].

[14] The conclusion from Figure 2 is that zonal variability of SCO in the low-latitude tropics is acceptably small at a few DU for calculating TCO maps from the CCD method, whereas it becomes unsuitably large when extending outside the tropics. The indicated time series mean and RMS  $\sim 0$ – $2$  DU in low latitudes (Figure 2 top) are both noise level. (We attribute “noise level” subjectively as no more than 5 DU for both TCO and SCO measurements.) However, an RMS of 12.6 DU for  $20^\circ\text{N}$ – $30^\circ\text{N}$  (Figure 2 bottom) is not noise level, and further indicates the presence of an annual cycle, with the largest Atlantic/Pacific differences in winter and spring months.

[15] Figure 3 compares SCO time series from CCD and SAGE outside the tropics at selected latitudes, both in the NH (left plots) and Southern Hemisphere (SH) (right plots). The comparison is made for the 1984 to 2003 time period as in Figure 1. Also, as in Figure 1, “zonal average” in Figure 3 for CCD measurements refers to averaging only over the Pacific about the dateline from  $120^\circ\text{W}$  to  $120^\circ\text{E}$ . For SAGE it means at least 10 profile measurements per month in a given  $5^\circ$  latitude band (neither measurement is a true zonal mean). Figure 3 suggests that even outside the tropics, CCD SCO evaluated from only the Pacific region simulates the annual cycle of SCO inferred from the SAGE data. The left plots for the NH suggest that the SCO measurements from CCD can be extended to high latitudes ( $50^\circ\text{N}$ – $60^\circ\text{N}$ ). For the SH (right plots), CCD SCO measurements become scarce poleward of  $\sim 50^\circ\text{S}$  because of a low occurrence rate of convective clouds. We note that there may be considerable temporal and spatial variability in SCO outside tropical latitudes, particularly in winter and spring, caused by large-scale planetary waves and baroclinic waves. The monthly averaging over the Pacific largely smoothes variability in CCD SCO. It is emphasized that measurements of SCO from the CCD method are a representation of only the broad Pacific region as a function of latitude and month.

[16] Table 1a summarizes the comparison statistics of SCO derived from the SAGE and CCD time series for  $60^\circ\text{S}$  to  $60^\circ\text{N}$ . Statistical comparisons also include the tropical latitudes shown in Figure 1. Table 1a indicates relatively larger offset differences and larger RMS values at middle and high latitudes than in the tropics even though the

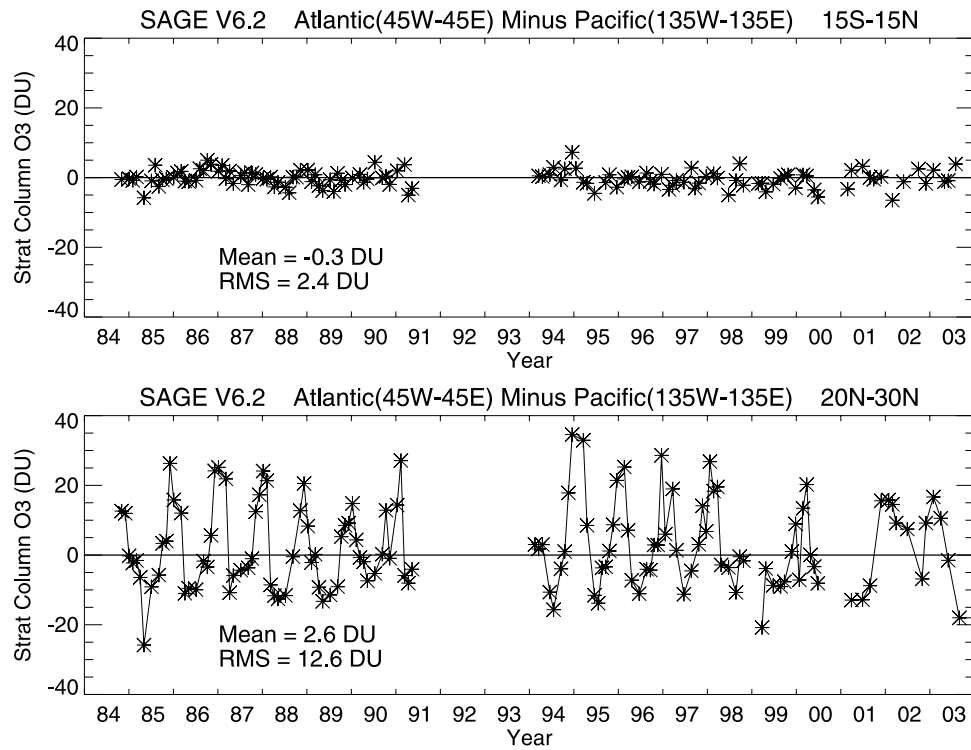


**Figure 2.** (top) Difference of Atlantic ( $45^{\circ}\text{W}$ – $45^{\circ}\text{E}$ ) minus Pacific ( $135^{\circ}\text{W}$ – $135^{\circ}\text{E}$ ) SAGE II SCO (in DU) averaged over latitudes  $15^{\circ}\text{S}$  to  $15^{\circ}\text{N}$ . (bottom) Same as top frame but for the latitude band  $20^{\circ}\text{N}$  to  $30^{\circ}\text{N}$ . Time series averages and RMS amplitudes are indicated. A constraint is that there must be at least five SAGE II profile measurements per latitude band for each monthly ensemble average.

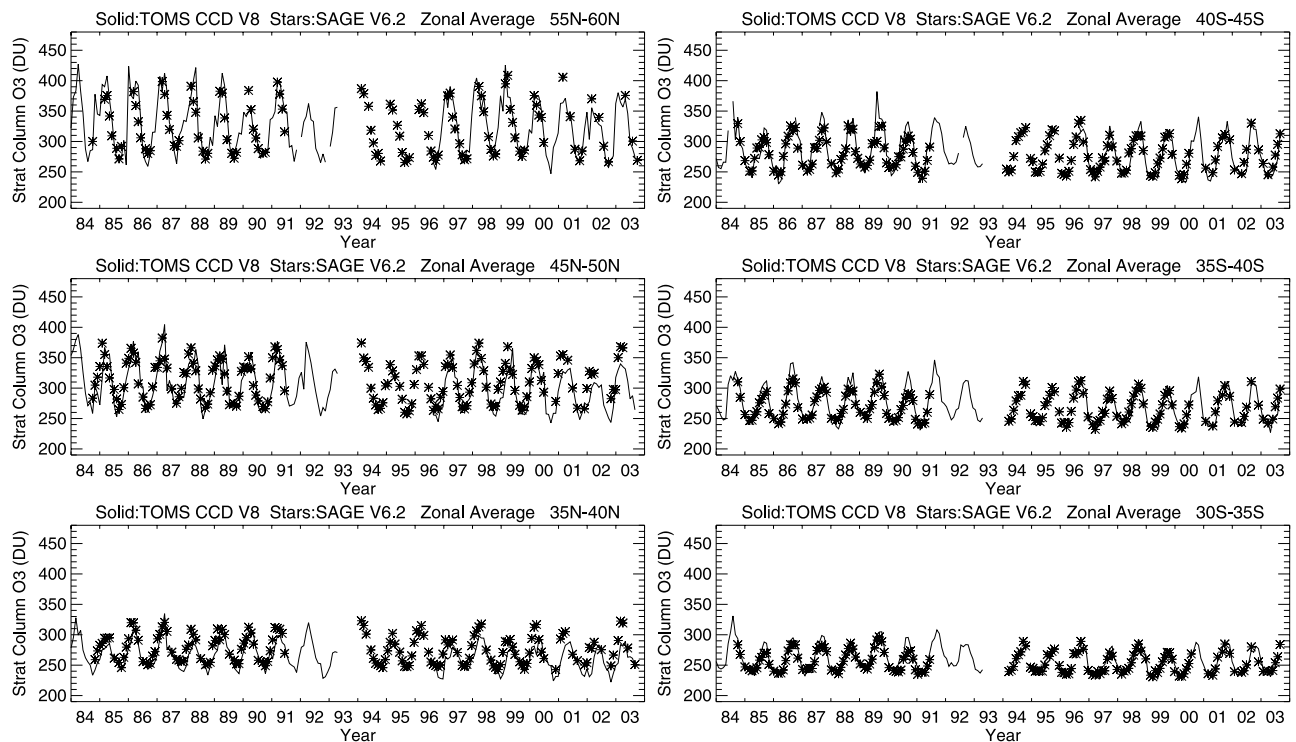


**Figure 3.** Time series comparisons (in DU) between SAGE II SCO (stars) and TOMS CCD SCO (solid curves) outside the tropics at midlatitudes in the (left) Northern Hemisphere and (right) Southern Hemisphere.

**Table 1b.** Same as Table 1a but for Summertime Months Only<sup>a</sup>

Latitude	<i>N</i>	Diff, DU	RMS, DU	<i>r</i>
55°N–60°N	24	2.9	18.4	0.88
50°N–55°N	28	2.0	17.8	0.80
45°N–50°N	23	4.5	20.6	0.78
40°N–45°N	21	0.8	8.9	0.84
35°N–40°N	19	1.7	5.0	0.87
30°N–35°N	19	0.9	2.4	0.94
25°N–30°N	18	3.4	5.7	0.81
20°N–25°N	17	5.2	7.1	0.81
15°N–20°N	16	3.8	6.1	0.45
10°N–15°N	16	0.4	3.0	0.77
5°N–10°N	17	−3.5	4.5	0.90
0°–5°N	22	−2.4	4.1	0.91
0°–5°S	22	−3.4	4.3	0.96
5°S–10°S	18	−1.9	3.1	0.92
10°S–15°S	18	−0.9	2.3	0.93
15°S–20°S	18	−0.4	3.0	0.90
20°S–25°S	18	1.8	3.8	0.87
25°S–30°S	18	3.0	6.1	0.74
30°S–35°S	19	3.6	6.2	0.81
35°S–40°S	18	3.6	6.6	0.80
40°S–45°S	20	0.8	6.8	0.77
45°S–50°S	25	0.6	11.5	0.70
50°S–55°S	27	−3.9	16.2	0.52
55°S–60°S	23	−2.4	17.1	0.62

<sup>a</sup>Summertime months are June, July, and August for the Northern Hemisphere and December, January, and February for the Southern Hemisphere.

two time series are highly correlated over most of the latitude range. The differences in the extratropics may be a manifestation of differing temporal and spatial data sampling, especially during winter and spring months when SCO variability is driven largely by planetary-scale waves and baroclinic waves. During summer months, SCO exhibits much less temporal and spatial variability. Table 1b shows a similar comparison between TOMS and SAGE SCO but only for summer months (June–August for the NH and December–February for the SH). Table 1b shows noise-level offset differences (i.e., no more than 5 DU) for all latitudes and RMS differences less than 10 DU out to 45° latitude in both summer hemispheres. Large RMS differences may be due to dynamical forcing of SCO coupled with the low sampling rates of only a few daily measurements per month.

[17] Filtering SAGE data for Pacific-only averaging tends to increase rather than decrease offset and RMS difference values in Table 1a because of low SAGE sampling rates when only one third of the longitude range is considered. Since clouds are generally lower than the tropopause height, the CCD method will tend to overestimate rather than underestimate SCO. The negative bias in Table 1a at NH midlatitudes is probably due to overestimation of SCO from SAGE. Tropopause height, which is highly variable during winter and spring months in middle and high latitudes [e.g., Logan *et al.*, 1999], can significantly affect the calculation of SCO from SAGE profile measurements. Tropopause height uncertainties in these months may attribute to some of the offset differences seen in Table 1a.

[18] Figure 4 shows time series comparisons of USCO (top curves in each plot) and LSCO (bottom curves) with SAGE for the same latitude bands shown in Figure 3. A constant 200 DU was added to the USCO time series in Figure 4 to separate it from the LSCO series for visual

comparison. TOMS/SBUV USCO in Figure 4 tends to be lower by about 4–5 DU on average, compared to SAGE USCO, while RMS differences are ~5–6 DU. These numbers are persistent for USCO and apply for all latitudes from 60°S to 60°N. For LSCO (bottom curves), TOMS/SBUV is lower than SAGE by around 7 DU on average with RMS differences of ~10–20 DU for latitudes 60°S to 60°N. Tables 2a and 2b summarize statistical comparisons for the USCO and LSCO time series, respectively, plotted in Figure 4. As in Tables 1a and 1b, comparisons are listed for all latitude bands from 60°S to 60°N. Because of large seasonal cycles present, correlations between time series of either USCO or LSCO vary from around 0.7 to 0.9.

[19] The comparison of stratospheric ozone time series derived from the CCD method with SAGE measurements shows that CCD-derived products from TOMS and SBUV can be used to supplement SAGE data as a long-record data field in the tropics extending to middle and high latitudes over the Pacific. Both SCO (including USCO and LSCO) and TCO time series have been generated for 1979–2003 using the CCD method. An analysis of these time series involving seasonal cycles and trends is presented in sections 6 and 7.

## 5. CCD and Ozone Sonde TCO Comparisons

[20] It is interesting to note that while SCO in the tropics from the CCD method agrees remarkably well with SAGE over the long time record, TCO from the CCD method also agrees well with ozonesonde TCO in the tropics. Figure 5a shows CCD-derived TCO time series from 1984 to 2003 at four tropical locations. These locations correspond to Southern Hemisphere additional ozonesondes (SHADOZ) sites where TCO data from ozonesondes overlap with TOMS measurements for several years [Thompson *et al.*, 2003]. Because of the zonal invariance of SCO in the tropics the TCO at any location in the tropics can be estimated by taking the difference of low-reflectivity ( $R < 0.2$ ) TOMS total column ozone at that location and SCO estimated from the high reflecting ( $R > 0.9$ ) convective clouds in the Pacific at a similar latitude. Ozonesonde TCO represents monthly ensemble averages, often composed of about four measurements per month. All of the sites except Natal (5°S, 35°W) include additional measurements prior to the official beginning of the SHADOZ network (January 1998). In Figure 5a, Nairobi, near the equator on the east coast of Africa, shows small variability in TCO when compared to the Atlantic sites of Ascension Island and Natal. Watukosek in the western Pacific also has a weak seasonal cycle. It, however, shows large increases in TCO during the recent El Niño events of 1997–1998 [Chandra *et al.*, 1998, 2002] and 2002. Table 3 summarizes statistical comparisons between TOMS and SHADOZ TCO from Figure 5a. On average, TOMS TCO is ~1 DU more than SHADOZ TCO, while RMS differences are ~4–5 DU. Correlations between TOMS and SHADOZ TCO time series vary from about 0.7 to 0.8.

[21] Unlike the low-latitude tropics, the assumption of zonal invariance of SCO cannot be made outside the latitude range 15°N and 15°S. Therefore the comparison between CCD and ozonesonde TCO measurements outside the tropics can only be made in the Pacific region. We have

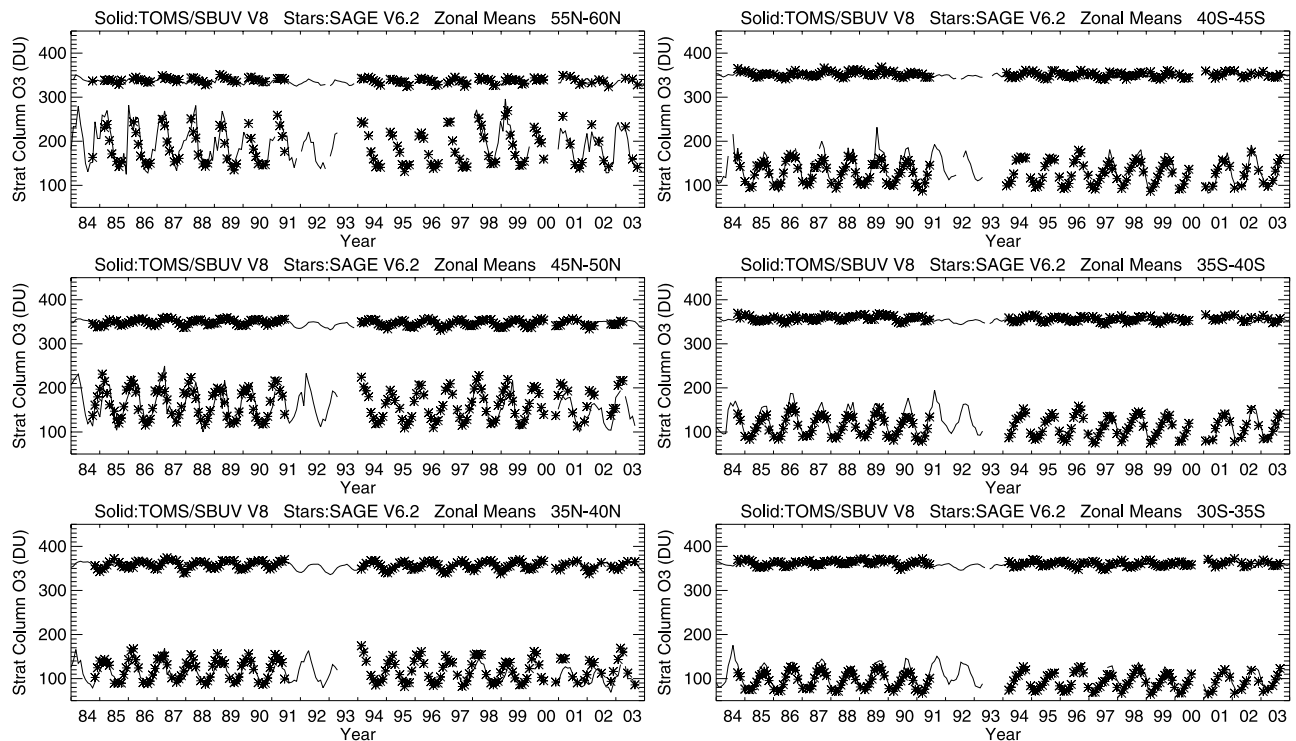


**Figure 4.** Similar to Figure 3 but within each frame is a comparison of upper stratospheric column ozone (USCO) (top two time series in each plot) and lower stratospheric column ozone (LSCO) (bottom two time series in each plot): SAGE II time series (stars) and USCO from solar backscatter ultraviolet (SBUV) and LSCO from TOMS/SBUV (solid curves). A constant of 200 DU was added to all USCO time series to separate them from LSCO time series for visual comparisons. Column amounts are in DU. SBUV and SAGE measurements include all available data along longitude (i.e., zonal mean).

**Table 2a.** Same as Table 1a but for USCO From SBUV and SAGE<sup>a</sup>

Latitude	<i>N</i>	Diff, DU	RMS, DU	<i>r</i>
55°N–60°N	87	–2.7	3.8	0.88
50°N–55°N	109	–2.9	4.1	0.83
45°N–50°N	128	–2.8	3.7	0.91
40°N–45°N	122	–3.5	4.4	0.92
35°N–40°N	120	–3.8	4.7	0.94
30°N–35°N	117	–3.7	4.6	0.95
25°N–30°N	116	–3.6	4.6	0.95
20°N–25°N	112	–3.7	4.8	0.93
15°N–20°N	101	–4.3	5.1	0.93
10°N–15°N	92	–5.6	6.1	0.91
5°N–10°N	82	–5.8	6.6	0.79
0°–5°N	87	–5.2	6.3	0.75
0°–5°S	83	–5.0	6.2	0.74
5°S–10°S	86	–4.8	5.6	0.76
10°S–15°S	98	–4.7	5.4	0.86
15°S–20°S	107	–4.8	5.6	0.87
20°S–25°S	111	–4.6	5.5	0.86
25°S–30°S	118	–4.9	5.8	0.86
30°S–35°S	117	–5.1	5.9	0.85
35°S–40°S	117	–5.3	6.1	0.84
40°S–45°S	116	–4.9	6.0	0.82
45°S–50°S	122	–4.0	5.3	0.85
50°S–55°S	103	–4.4	5.6	0.86
55°S–60°S	83	–4.1	5.7	0.83

<sup>a</sup>Definitions are USCO, upper stratosphere column ozone; and SBUV, solar backscatter ultraviolet. Diff is SBUV minus SAGE.

**Table 2b.** Same as Table 1a but for LSCO From TOMS/SBUV and SAGE<sup>a</sup>

Latitude	<i>N</i>	Diff, DU	RMS, DU	<i>r</i>
55°N–60°N	76	7.6	23.7	0.87
50°N–55°N	98	–0.8	22.6	0.81
45°N–50°N	117	–5.2	24.2	0.76
40°N–45°N	111	–8.2	20.1	0.82
35°N–40°N	110	–9.1	16.6	0.81
30°N–35°N	108	–5.3	10.7	0.78
25°N–30°N	106	0.8	7.9	0.75
20°N–25°N	95	3.5	8.5	0.80
15°N–20°N	75	5.5	8.6	0.67
10°N–15°N	58	4.2	6.1	0.73
5°N–10°N	46	1.9	4.0	0.78
0°–5°N	52	1.9	3.6	0.79
0°–5°S	52	1.4	3.9	0.68
5°S–10°S	52	0.0	3.1	0.51
10°S–15°S	69	0.2	3.9	0.40
15°S–20°S	85	2.8	6.3	0.70
20°S–25°S	102	6.9	9.5	0.83
25°S–30°S	109	9.5	11.4	0.91
30°S–35°S	110	9.8	12.8	0.93
35°S–40°S	110	8.9	14.8	0.91
40°S–45°S	107	7.8	18.4	0.86
45°S–50°S	103	6.2	21.8	0.77
50°S–55°S	71	10.4	29.1	0.70
55°S–60°S	60	12.3	30.0	0.57

<sup>a</sup>Abbreviations are LSCO, lower stratospheric column ozone; and Diff, TOMS/SBUV minus SAGE.



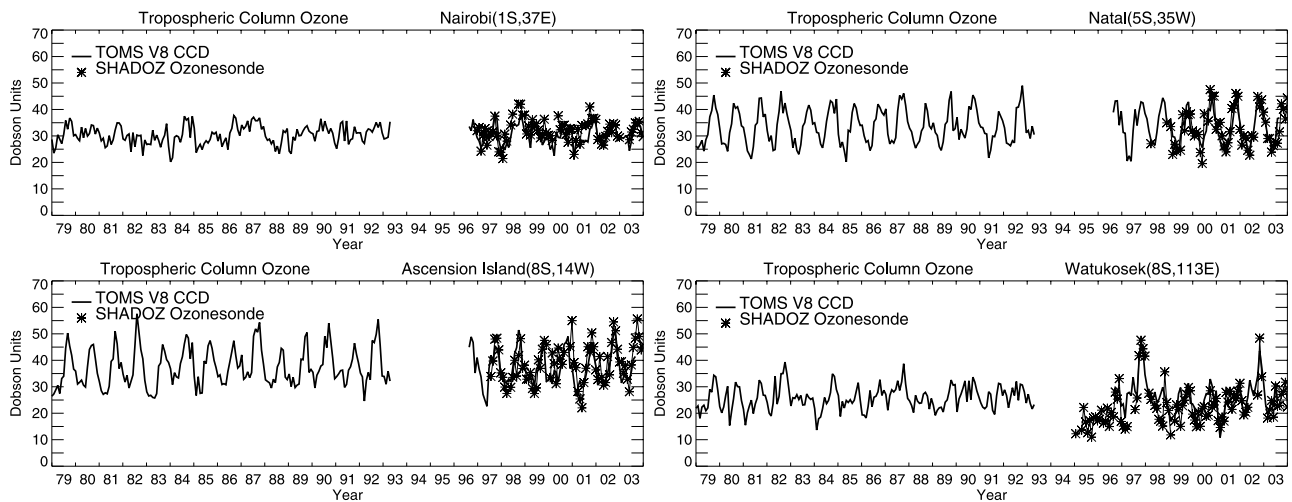


**Figure 5a.** Time series comparisons of tropospheric column ozone (TCO) (in DU) between CCD (solid curves) and ozonesonde (stars) at four Southern Hemisphere additional ozonesondes (SHADOZ) sites: (top left) Nairobi (1°S, 37°E); (top right) Natal (5°S, 35°W); (bottom left) Ascension Island (8°S, 14°W); and (bottom right) Watukosek (8°S, 113°E).

estimated SCO for a few available ozonesonde sites outside low latitudes in the Pacific by averaging CCD SCO measurements over a broad region (5° latitude by 25° longitude) centered about each site. This generally yields enough data points to provide an estimation of SCO at a given ozonesonde site.

[22] Figure 5b compares TCO between CCD and ozonesondes at four Pacific stations lying outside the

low-latitude tropics. Figure 5b also shows TCO seasonal cycles determined from the TOMS and SAGE residual method [Fishman *et al.*, 1990, 1992; Fishman and Brackett, 1997]. SAGE SCO was averaged for the same 5° latitude by 25° longitude region centered around each site as for the CCD SCO. SAGE TCO seasonal cycles in Figure 5b were determined using data from 1984–2003, while CCD used 1979–2003. For ozonesondes the years

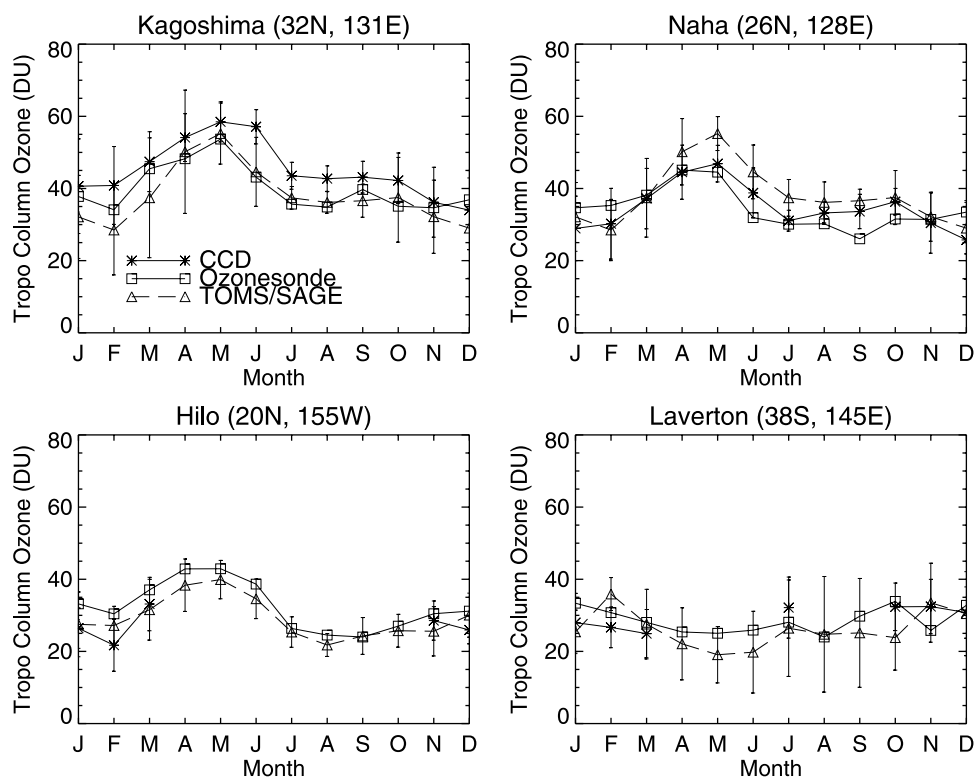


**Figure 5b.** Time series comparisons of TCO (in DU) between CCD (stars), ozonesonde (squares), and TOMS/SAGE (triangles) at four Pacific sites: (top left) Kagoshima (32°N, 131°E); (top right) Naha (26°N, 128°E); (bottom left) Hilo (20°N, 155°W); and (bottom right) Laverton (38°S, 145°E).



**Table 3.** Statistical Measurements of TOMS/SHADOZ (Similar to Tables 1 and 2) for the Time Series Plotted in Figure 5a<sup>a</sup>

Station	<i>N</i>	Diff, DU	RMS, DU	<i>r</i>
Nairobi	71	−1.7	3.7	0.65
Natal	55	0.0	3.9	0.83
Watuikosek	73	2.0	5.0	0.79
Ascension	70	−1.2	5.5	0.67

<sup>a</sup>Definitions are SHADOZ, Southern Hemisphere additional ozonesondes; TCO, tropospheric column ozone; and Diff, TOMS minus SHADOZ.

included were 1979–2000. The largest annual mean offset difference in TCO between CCD and ozonesondes is 5 DU for Kagoshima (with CCD larger); for TOMS/SAGE and ozonesondes it is 4 DU for Naha (with TOMS/SAGE larger).

[23] The mean seasonal cycle pattern agrees reasonably well at each station site in Figure 5b. Laverton in the SH indicates a weak seasonal cycle, while the Japanese stations and also Hilo, all NH sites, show a distinct seasonal pattern with the largest TCO around late spring (~April–May). This late spring maximum agrees with the ozonesonde profile seasonal cycles shown by *Naja and Akimoto* [2004, Figure 2] for Kagoshima and Naha.

## 6. Seasonal Variation in Total Column Ozone, SCO, LSCO, USCO, and TCO

[24] Figure 6 depicts seasonal variability of CCD SCO and total column ozone for the Pacific region based on

all available data from 1979–2003. Because most ozone lies in the stratosphere, stratospheric column ozone and total column ozone exhibit similar seasonal cycles and latitudinal variability. The largest column amounts in either hemisphere occur during winter–spring months and coincide with a lowering of the tropopause. The seasonal characteristics of total column and stratospheric column ozone are discussed extensively in the literature and are similar to those given in Figure 6 [e.g., *World Meteorological Organization (WMO)*, 1990, and references therein; *Stratospheric Processes and Their Role in Climate (SPARC)*, 1998, and references therein; *Fortuin and Kelder*, 1998, and references therein]. The climatological features of total and stratospheric column ozone in the Pacific region are similar to those inferred from the zonally averaged climatology inferred from earlier versions of TOMS and SAGE data (see, e.g., Figure 3.48 of *SPARC* [1998], which is based on data from TOMS total ozone (version 7 for 1979–1994) and SAGE I/II (version 5.96 for 1979–1996)).

[25] Figure 7 shows seasonal variability in USCO (top) and LSCO (bottom) in the tropics. USCO shows weaker seasonality and weaker latitude dependence compared to LSCO. USCO in tropical latitudes is largest (~170 DU) compared to LSCO (~70 DU). In the extratropics the largest ozone amounts (~200–250 DU) occur in winter–spring months in the lower stratosphere. Latitudinal gradients in column ozone are opposite in sign between USCO and LSCO. Ozone is seen to decrease with latitude in both hemispheres for the upper stratosphere, while it increases

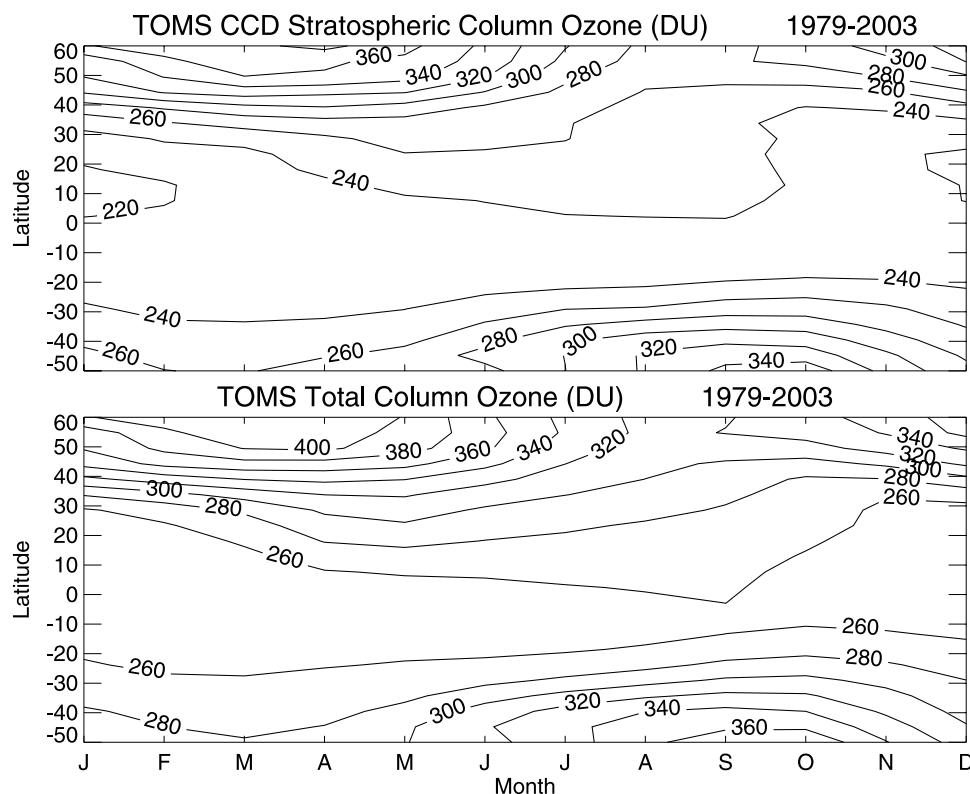


**Figure 6.** (top) Seasonal cycles in CCD SCO and (bottom) total column ozone derived from standard climatology calculation (all similar months averaged together). Ozone columns (in DU) are averaged over the eastern and western Pacific (120°W to 120°E).

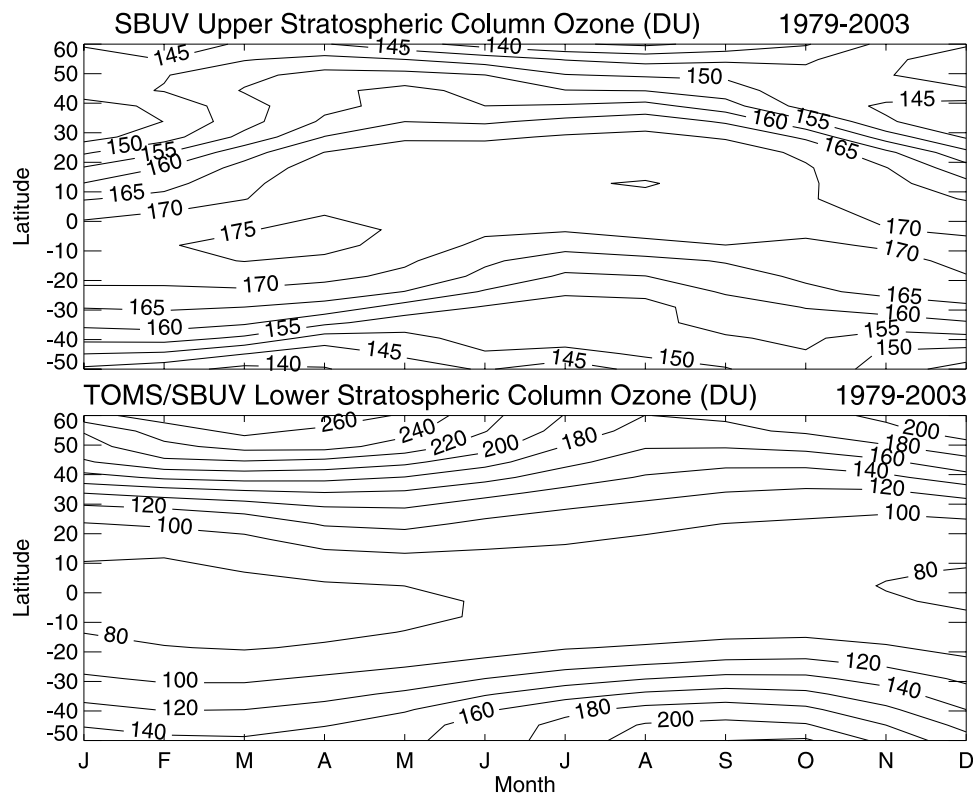


**Figure 7.** Similar to Figure 6 but with (top) USCO and (bottom) LSCO shown.

with latitude for the lower stratosphere. Latitudinal gradients are  $\sim 3$ – $4$  times larger for LSCO. Despite the differences in latitudinal gradients, USCO and LSCO in both hemispheres exhibit the largest amounts in winter–spring months.

[26] An important result from this study is the evaluation and characterization of Pacific TCO. Figure 8 shows seasonal variability in TCO. TCO is smallest in low latitudes ( $\sim 15$ – $20$  DU) and largest in NH midlatitudes ( $\sim 45$ – $50$  DU). TCO in the NH midlatitudes is significantly larger on average than in the SH. TCO in the extratropical SH is around  $25$ – $30$  DU, which is about 60% the column amount in the NH. TCO in the NH is largest around April in the

tropics and subtropics and largest in May–June in midlatitudes. TCO in the SH is largest around September–October over much of the latitude range.

## 7. Ozone Trends

[27] Our understanding of long-term changes in stratospheric ozone is based on the analysis of satellite data such as Nimbus 7 TOMS and SBUV, EP TOMS, SAGE, and SBUV/2 instruments on NOAA satellites. These data have been updated several times because of the changes in retrieval algorithms. As a result, a large number of papers have been published in the literature relating to ozone trends

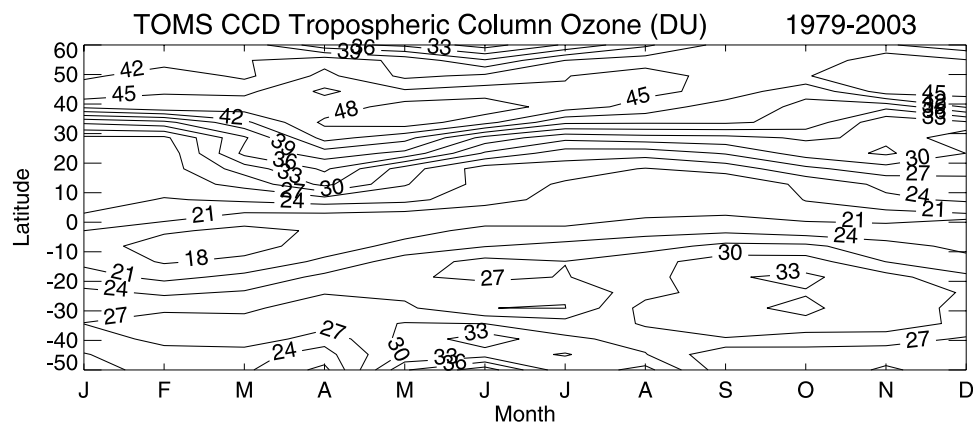


**Figure 8.** Similar to Figure 7 but for TOMS TCO.

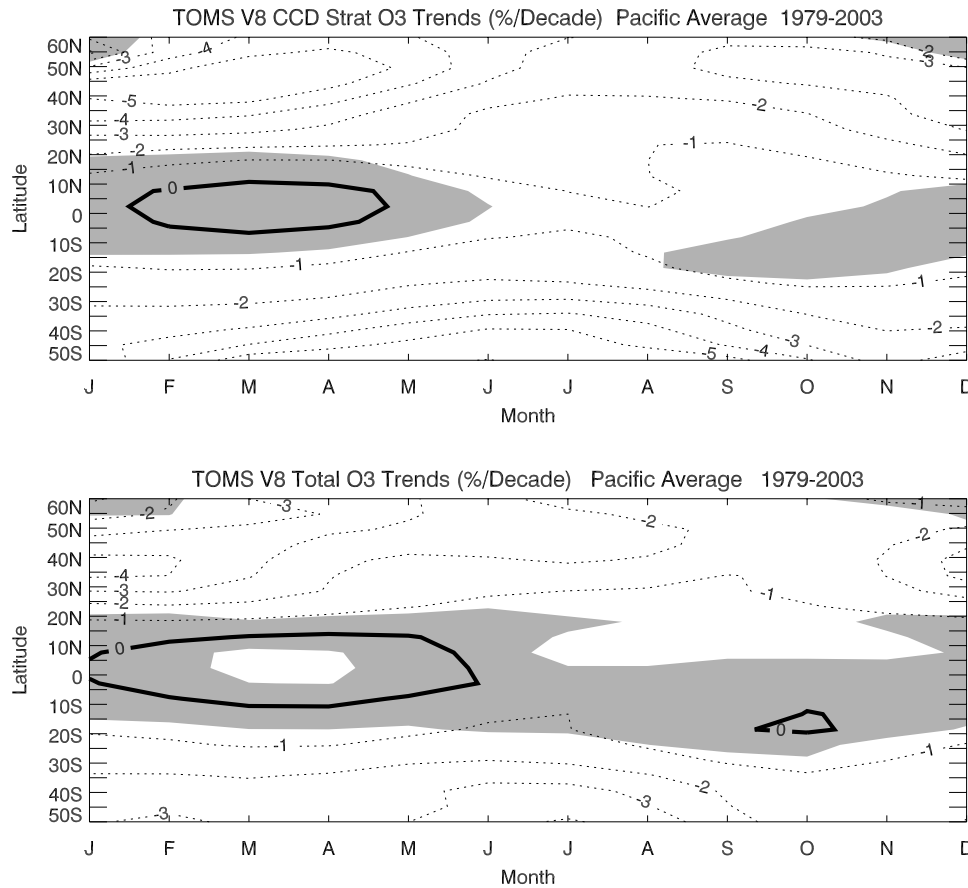


**Figure 9a.** Seasonal trends in (top) CCD SCO and (bottom) total column ozone derived from trend model (1). Ozone columns are averaged over the east-west Pacific, and trend units are in  $\% \text{ decade}^{-1}$ . Shaded regions depict trends that are not different from zero at the  $2\sigma$  statistical level.

in the stratosphere using different versions as discussed in several international reports on scientific assessment of ozone depletion [e.g., WMO, 2003, and references therein; SPARC, 1998]. Specific studies, to name a few, include Chandra and Stolarski [1991], Stolarski et al. [1991], Hood et al. [1993], Randel and Cobb [1994], Chandra et al. [1995], Hollandsworth et al. [1995], Jackman et al. [1996], Solomon et al. [1996], Miller et al. [1996], McPeters et al. [1996], Ziemke et al. [1997], Cunnold et al. [2000], Li et al. [2002], Weatherhead et al. [2000], Reinsel et al. [2002], and Newchurch et al. [2003].

[28] In this section we describe ozone trends in the different regions of the atmosphere in the Pacific region using TOMS and SBUV measurements. These trends were determined using a statistical regression model [e.g., Stolarski et al., 1991; Randel and Cobb, 1994; Ziemke et al., 1997]:

$$\Omega(t) = A(t) + B(t)t + C(t)\text{QBO}(t) + D(t)\text{Solar}(t) + R(t). \quad (1)$$

In (1),  $t$  is the month index (1–300 for 1979–2003),  $\Omega(t)$  is column ozone,  $A(t)$  is the seasonal cycle coefficient,  $B(t)$  is the seasonal trend coefficient,  $C(t)$  is the seasonal QBO coefficient,  $D(t)$  is the seasonal solar cycle coefficient, and  $R(t)$  is the residual error time series for the regression model. Seasonal coefficients  $A(t)–D(t)$  in (1) are all 12-month

(modular) seasonal cycle derivations.  $A(t)$  involves seven fixed constants, and  $B(t)–D(t)$  involve five constants.  $A(t) = a(0) + \sum_{j=1}^3 [a(j)\cos(2\pi jt/12) + b(j)\sin(2\pi jt/12)]$ , where  $a$  and  $b$  are constants, with a similar form for coefficients  $B(t)–D(t)$ . The trend coefficient  $B(t)$  in (1) includes an additional  $1\% \text{ decade}^{-1}$  multi-instrument uncertainty in all measurements for the 1979–2003 time period. The largest interannual correlations between Singapore ( $1^\circ\text{N}$ ,  $140^\circ\text{E}$ ) winds and all five column amounts listed above were either at 30 hPa or 40 hPa; for consistency, QBO( $t$ ) in (1) for all sources of  $\Omega(t)$  was taken as 30 hPa Singapore monthly zonal winds. Solar( $t$ ) in (1) was taken as 10.7 cm solar flux (F10.7) monthly mean time series. Phase lags were not applied to either QBO( $t$ ) or Solar( $t$ ).

[29] The regression model (1) was implemented individually for each of the five column ozone quantities listed in section 1. All column ozone data in (1) represent zonal averages of Pacific measurements about the dateline from  $120^\circ\text{W}$  to  $120^\circ\text{E}$ . Because of insufficient numbers of CCD measurements poleward of  $50^\circ\text{S}$  and  $60^\circ\text{N}$  for deriving seasonal coefficients, all analyses using (1) were applied to the latitude range  $50^\circ\text{S}$  to  $60^\circ\text{N}$ . The trend model (1) was also applied to TCO with an additional southern oscillation index El Niño proxy term, which was found to have no significant impact in altering the derived seasonal cycles and trends.

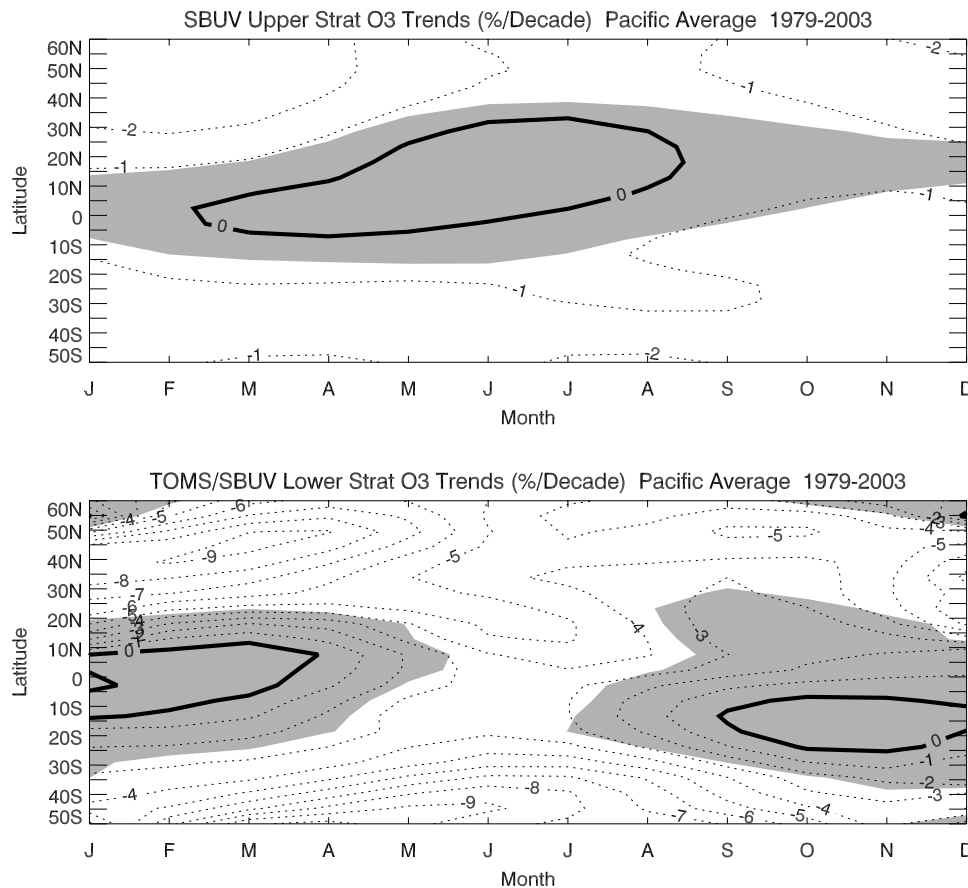


**Figure 9b.** Similar to Figure 9a but for (top) SBUV USCO and (bottom) TOMS/SBUV LSCO.

### 7.1. Seasonal Trends in Total Column Ozone, SCO, LSCO, and USCO

[30] Our investigation of ozone trends begins with SCO and total column ozone for 1979–2003. In Figure 9a, seasonal trends ( $\% \text{ decade}^{-1}$ ) are compared between SCO (top plot) and TOMS total column ozone (bottom plot). For the  $50^{\circ}\text{S}$ – $60^{\circ}\text{N}$  latitude range the largest decreases in total column ozone occur in the NH around  $40^{\circ}\text{N}$ – $50^{\circ}\text{N}$  in winter and spring months with trend values in the range of  $4$ – $5\% \text{ decade}^{-1}$ . In the SH the largest decreases in column ozone are around  $40^{\circ}\text{S}$ – $50^{\circ}\text{S}$  in June–July (southern winter) with trend values comparable to those in the NH. The seasonal trends in SCO are similar to those in total column ozone. However, the SCO trends in the extratropics of both hemispheres are  $\sim 1\% \text{ decade}^{-1}$  more negative than trends in total column ozone, suggesting possible increases in TCO. The seasonal characteristics of column ozone trends in Figure 9a are similar to those first reported by Stolarski *et al.* [1991] based on TOMS version 6 column ozone data from 1979 to 1991. Their trend values were about 2–3% more negative than the values shown in Figure 9a.

[31] USCO and LSCO trends ( $\% \text{ decade}^{-1}$ ) are shown in Figure 9b. Because LSCO and USCO amounts in the extratropics are comparable (e.g., Figure 7), Figure 9b suggests a significantly larger depletion of ozone in the lower stratosphere outside the tropics than in the upper stratosphere. The seasonal variability in LSCO trends is

consistent with the ozonesonde results of Logan *et al.* [1999], which indicated that most of the seasonal variability of trends in extratropical SCO is credited to the lowermost part of the stratosphere between around 250 and 90 hPa (i.e., around 10 to 17 km). Figure 9b also indicates that the midlatitude minimum in total column ozone trends at around  $40^{\circ}\text{N}$ – $50^{\circ}\text{N}$  in winter–spring months is a feature generated primarily by ozone depletion in the lower stratosphere below 30 hPa. This feature is most likely of dynamical origin as discussed in a number of papers [e.g., Chandra *et al.*, 1996; Ziemke *et al.*, 1997; Hood *et al.*, 1997].

### 7.2. Comparison of Pacific Trends and Zonal Mean Trends

[32] The ozone trends in Figures 9a and 9b were derived from data in the Pacific region. They are not substantially different from the zonal mean trends as shown in Figure 10. The seasonally varying trends and trend uncertainties shown in Figure 9a are plotted in Figure 10 as annual mean values as a function of latitude. The trends are in physical units of  $\text{DU decade}^{-1}$  instead of  $\% \text{ decade}^{-1}$ . Also shown in Figure 10 are zonal mean trends (i.e., all longitudes included in the zonal average) in total column ozone. It is seen that the trends in total column ozone derived from the Pacific region are nearly identical with zonal mean trends, differing at most by  $1 \text{ DU decade}^{-1}$  over the entire latitude range. This suggests that Pacific-averaged total ozone



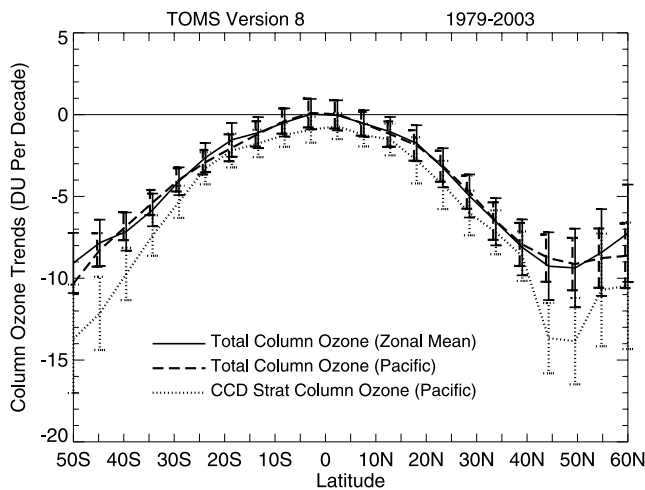


**Figure 10.** Annually averaged values of Pacific mean total column ozone trends (dashed line) and SCO trends (dotted curve) with trend  $\pm 2\sigma$  uncertainties from Figure 9a. Also shown are trends for zonal mean total ozone (solid curve). Trends are plotted in  $\text{DU decade}^{-1}$  rather than  $\% \text{ decade}^{-1}$ , as shown in Figure 9a. Time record for calculations is 1979–2003.

simulates the trends in zonal mean total ozone. As SCO makes up most of total column ozone, Pacific-averaged SCO from the CCD method (dotted curve in Figure 10) may then have trend features similar to true zonal mean SCO.

[33] As in Figure 9a, SCO trends in Figure 10 are more negative than total ozone trends at midlatitudes. These differences imply a positive trend in TCO in midlatitudes (discussed in section 7.3). We note that the EP TOMS version 8 data spanning 2001–2003 exhibit a potential instrument/algorithm artifact, which appears to affect mostly ozone measurements at high latitudes (R. D. McPeters and G. J. Labow, personal communication, 2004). To investigate this possible artifact and its impact on trends, we repeated our trend analyses for the 1979–2000 period. The removal of the 2001–2003 data had no substantial impact on the long-term trend results in Figures 9 and 10.

### 7.3. Annual Mean Trends in USCO, LSCO, and TCO

[34] Annual mean trends in USCO and LSCO for the 1979–2003 period are shown in Figure 11. The USCO trends are generally small ( $\sim -1$  to  $-3 \text{ DU decade}^{-1}$ ) over all latitudes between  $50^\circ\text{S}$  and  $60^\circ\text{N}$ . In contrast, LSCO trends change rapidly from around  $-1$  to  $-3 \text{ DU decade}^{-1}$  at low latitudes to about  $-10$  to  $-12 \text{ DU decade}^{-1}$  at middle-to-high latitudes. It is interesting to note that most ozone loss in the extratropics since 1979 has occurred in LSCO with  $\sim 3$ – $4$  times greater ozone loss than in USCO.

[35] The possibility of positive trends in TCO in the extratropics was indicated by Figures 9a and 10. Previous trend studies involving extratropical TCO have been limited to tropospheric ozone measurements from ozonesondes. The nature of TCO trends derived from ozonesonde measurements from 1980 to 2000 is that of high variability from station to station [e.g., Tarasick et al., 1995; Oltmans et al., 1998; Logan et al., 1999] and is discussed in the WMO [2003] report. The results from the WMO analyses indicated

statistically insignificant trends for most stations and zero trend when averaged over all midlatitude stations. In contrast, TCO for 1979–2003 in Figure 12 shows trends varying from zero in the tropics to about  $+2$  to  $+3 \text{ DU decade}^{-1}$  in the midlatitudes of both hemispheres. The  $2$ – $3 \text{ DU decade}^{-1}$  positive trends in Figure 12 correspond to around  $5$ – $8 \text{ DU}$  increases in TCO over the 25-year record. A recent study by Naja and Akimoto [2004] indicates substantial increases in TCO over Japan ozonesonde sites in the Pacific for the 1970–2002 time record (e.g., their Figure 2). Their study corroborates the positive trend results in Figure 12 for the NH Pacific midlatitudes.

[36] The nearly zero trend in the tropics is a characteristic of all longitudes (not shown) and is consistent with the earlier estimates of trends in this region derived from TOMS version 7 data for 1979 to 1992 [Chandra et al., 1999; Thompson and Hudson, 1999]. It is in disagreement with the recent results of Lelieveld et al. [2004], which indicated a significant increase in near-surface ozone in the tropics. Their results were based on shipborne ozone measurements over the Atlantic Ocean from 1977 to 2002. Lelieveld et al. [2004, p. 1485] have attributed the disagreement with the TOMS measurements to “limited sensitivity of the TOMS measurements for lower tropospheric ozone, interference by clouds and aerosols, instrument discontinuities, and the difficulty of determining the location of the tropopause.”

[37] The TCO trends shown in Figure 12 are based on a much larger database than previous studies, including Lelieveld et al. [2004]. Some of the issues raised by Lelieveld et al. [2004] have been addressed in the version 8 algorithm. It is noted that the CCD method does not depend on the determination of either cloud height or tropopause height information to estimate TCO and that the efficiency correction for detecting ozone in the troposphere has been incorporated for characterizing the latitudinal and seasonal variability in TCO. The excellent agreement between CCD and ozonesonde TCO at Watukosek (Figure 5a) during this period suggests that the sensitivity of TOMS measurements in the lower troposphere is not affected

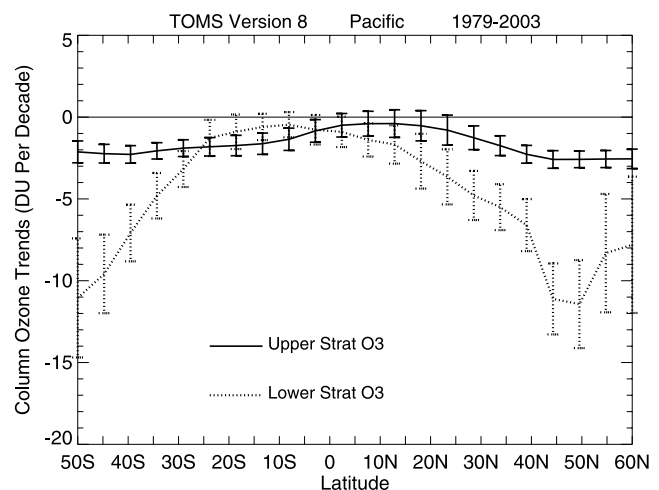


**Figure 11.** Annual mean trends and  $\pm 2\sigma$  trend uncertainties (vertical bars) for USCO (solid curve) and LSCO (dotted curve). Time period for trend analyses is January 1979 to December 2003. Values are in  $\text{DU decade}^{-1}$ .

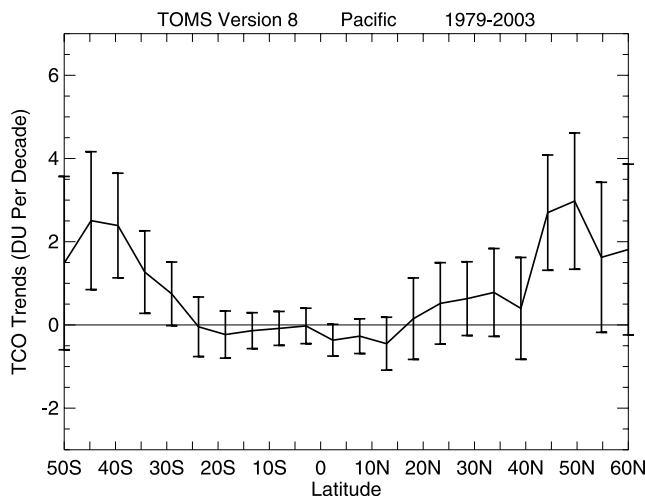


**Figure 12.** Annual average values of trends and trend  $\pm 2\sigma$  uncertainties in TCO for 1979–2003. Numbers are in DU decade<sup>-1</sup>.

seriously. The efficiency correction, however, does not account for interannual and long-term changes in boundary layer ozone. TCO derived from TOMS measurements may therefore not reflect such changes in boundary layer ozone. However, *Lelieveld et al.* [2004] have suggested that their observed trend in surface ozone is not a localized phenomenon since ozone and other trace constituents are efficiently transferred from the boundary layer to the middle and upper troposphere by deep convection. Our analysis of TCO trends in the tropics does not indicate a significant increase.

## 8. Summary

[38] By combining the newly processed TOMS CCD and SBUV version 8 data from 1979 to 2003, we have characterized the seasonal cycle, latitude dependence, and long-term trends in ozone in three broad layers of the atmosphere over the Pacific (averaged over 120°W–120°E): upper stratosphere (32 hPa and above), lower stratosphere (32 hPa to tropopause), and troposphere. The analyses show that seasonal variability and meridional gradients of upper stratospheric column ozone (USCO) are weak in all latitude ranges compared to lower stratospheric column ozone (LSCO). Meridional gradients are  $\sim 3$ –4 times larger for those in LSCO and are opposite in sign compared to USCO, where USCO is seen to decrease with latitude in both hemispheres.

[39] Our study has examined ozone trends for 1979–2003 in the upper and lower atmosphere over the Pacific from combined TOMS and SBUV measurements. Over this 25-year record most ozone depletion has occurred in the lower stratosphere below  $\sim 25$  km altitude. In middle and high latitudes the ozone losses are  $\sim 3$ –4 times larger in the lower stratosphere compared to the upper stratosphere, even though average column amounts are comparable in the two layers.

[40] Our trend analyses for 1979–2003 also indicate moderate increases in TCO of about 5–8 DU in the midlatitudes of both hemispheres. With an increase in

industrial pollution over the last 25 years it is plausible to anticipate such an increase in tropospheric ozone as indicated in several studies [e.g., *Lelieveld and Dentener*, 2000; *Hauglustaine and Brasseur*, 2001]. However, it is also possible that the increase in TCO in midlatitudes may be of dynamical origin, caused by long-term increases in stratosphere-troposphere exchange. Comparison of model results with satellite measurements of TCO suggest that both stratosphere-troposphere exchange and  $\text{NO}_x$  emissions associated with industrial pollution play important roles in controlling the distribution of tropospheric ozone in midlatitudes [*Chandra et al.*, 2004]. We note that the detected increase in Pacific-averaged TCO in the NH midlatitudes is supported in a recent study showing substantial increases in TCO for Japan ozonesonde stations for the 1970–2002 period.

[41] **Acknowledgments.** We wish to thank the TOMS ozone processing team for the version 8 data. We are particularly thankful to the late C. G. Wellemeyer for his outstanding contribution in producing the TOMS and SBUV version 8 data. We also wish to thank the NASA Langley Research Center and the NASA Langley Radiation and Aerosols Branch for providing the SAGE II version 6.2 data. We greatly appreciate the effort of the SHADOZ team, especially A. M. Thompson and J. C. Witte, for the extensive SHADOZ ozonesonde data. Funding for this research was provided by Goddard Earth Science Technology (GEST) grant NCC5-494.

## References

- Ahn, C., J. R. Ziemke, S. Chandra, and P. K. Bhartia (2003), Derivation of tropospheric column ozone from the Earth Probe TOMS/GOES co-located data sets using the cloud slicing technique, *J. Atmos. Sol. Terr. Phys.*, **65**(10), 1127–1137.
- Bhartia, P. K., C. G. Wellemeyer, S. L. Taylor, N. Nath, and A. Gopalan (2004), Solar Backscatter Ultraviolet (SBUV) version 8 profile algorithm, *Proc. Quadrenn. Int. Ozone Symp.*, **XX**, 295–296.
- Chandra, S., and R. S. Stolarski (1991), Recent trends in stratospheric total ozone: Implications of dynamical and El Chichon perturbations, *Geophys. Res. Lett.*, **18**(12), 2227–2280.
- Chandra, S., C. H. Jackman, and E. L. Fleming (1995), Recent trends in ozone in the upper stratosphere: Implications for chlorine chemistry, *Geophys. Res. Lett.*, **22**(7), 843–846.
- Chandra, S., L. Froidevaux, J. W. Waters, O. R. White, G. J. Rottman, D. K. Prinz, and G. E. Brueckner (1996), Ozone variability in the upper stratosphere during the declining phase of the solar cycle 22, *Geophys. Res. Lett.*, **23**(21), 2935–2938.
- Chandra, S., J. R. Ziemke, W. Min, and W. G. Read (1998), Effects of 1997–1998 El Niño on tropospheric ozone and water vapor, *Geophys. Res. Lett.*, **25**(20), 3867–3870.
- Chandra, S., J. R. Ziemke, and R. W. Stewart (1999), An 11-year solar cycle in tropospheric ozone from TOMS measurements, *Geophys. Res. Lett.*, **26**(2), 185–188.
- Chandra, S., J. R. Ziemke, P. K. Bhartia, and R. V. Martin (2002), Tropical tropospheric ozone: Implications for dynamics and biomass burning, *J. Geophys. Res.*, **107**(D14), 4188, doi:10.1029/2001JD000447.
- Chandra, S., J. R. Ziemke, and R. V. Martin (2003), Tropospheric ozone at tropical and middle latitudes derived from TOMS/MLS residual: Comparison with a global model, *J. Geophys. Res.*, **108**(D9), 4291, doi:10.1029/2002JD002912.
- Chandra, S., J. R. Ziemke, X. Tie, and G. Brasseur (2004), Elevated ozone in the troposphere over the Atlantic and Pacific oceans in the Northern Hemisphere, *Geophys. Res. Lett.*, **31**, L23102, doi:10.1029/2004GL020821.
- Cunnold, D. M., M. J. Newchurch, L. E. Flynn, H. J. Wang, J. M. Russell, R. McPeters, J. M. Zawodny, and L. Froidevaux (2000), Uncertainties in upper stratospheric ozone trends from 1979 to 1996, *J. Geophys. Res.*, **105**(D4), 4427–4444.
- Fishman, J., and V. G. Brackett (1997), The climatological distribution of tropospheric ozone derived from satellite measurements using version 7 Total Ozone Mapping Spectrometer and Stratospheric Aerosol and Gas Experiment data sets, *J. Geophys. Res.*, **102**(D15), 19,275–19,278.
- Fishman, J., C. E. Watson, J. C. Larsen, and J. A. Logan (1990), Distribution of tropospheric ozone determined from satellite data, *J. Geophys. Res.*, **95**(D4), 3599–3617.

- Fishman, J., V. G. Brackett, and K. Fakhruzzaman (1992), Distribution of tropospheric ozone in the tropics from satellite and ozonesonde measurements, *J. Atmos. Terr. Phys.*, **54**(5), 589–597.
- Fortuin, J. P. F., and H. Kelder (1998), An ozone climatology based on ozonesonde and satellite measurements, *J. Geophys. Res.*, **103**(24), 31,709–31,734.
- Hauglustaine, D. A., and G. P. Brasseur (2001), Evolution of tropospheric ozone under anthropogenic activities and associated radiative forcing of climate, *J. Geophys. Res.*, **106**(D23), 32,337–32,360.
- Hollandsworth, S. M., R. D. McPeters, L. E. Flynn, W. Planet, A. J. Miller, and S. Chandra (1995), Ozone trends deduced from combined Nimbus 7 SBUV and NOAA 11 SBUV/2 data, *Geophys. Res. Lett.*, **22**(8), 905–908.
- Hood, L. L., R. D. McPeters, J. P. McCormack, L. E. Flynn, S. M. Hollandsworth, and J. F. Gleason (1993), Altitude dependence of stratospheric ozone trends based on Nimbus 7 SBUV data, *Geophys. Res. Lett.*, **20**(23), 2667–2670.
- Hood, L. L., J. P. McCormack, and K. Labitzke (1997), An investigation of dynamical contributions to midlatitude ozone trends in winter, *J. Geophys. Res.*, **102**(D11), 13,079–13,093.
- Jackman, C. H., E. L. Fleming, S. Chandra, D. B. Considine, and J. E. Rosenfield (1996), Past, present, and future modeled ozone trends with comparisons to observed trends, *J. Geophys. Res.*, **101**(D22), 28,753–28,767.
- Lelieveld, J., and F. J. Dentener (2000), What controls tropospheric ozone?, *J. Geophys. Res.*, **105**(D3), 3531–3551.
- Lelieveld, J., J. van Aardenne, H. Fischer, M. de Reus, J. Williams, and P. Winkler (2004), Increasing ozone over the Atlantic Ocean, *Science*, **304**(5676), 1483–1487.
- Li, J., D. M. Cunnold, H.-J. Wang, E.-S. Yang, and M. J. Newchurch (2002), A discussion of upper stratospheric ozone asymmetries and SAGE trends, *J. Geophys. Res.*, **107**(D23), 4705, doi:10.1029/2001JD001398.
- Logan, J. A., et al. (1999), Trends in the vertical distribution of ozone: A comparison of two analyses of ozonesonde data, *J. Geophys. Res.*, **104**(D21), 26,373–26,399.
- McPeters, R. D., S. M. Hollandsworth, L. E. Flynn, J. R. Herman, and C. J. Seftor (1996), Long-term ozone trends derived from the 16-year combined Nimbus 7/Meteor 3 TOMS version 7 record, *Geophys. Res. Lett.*, **23**(25), 3699–3702.
- Miller, A. J., et al. (1996), Comparisons of observed ozone trends and solar effects in the stratosphere through examination of ground-based Umkehr and combined solar backscattered ultraviolet (SBUV) and SBUV 2 satellite data, *J. Geophys. Res.*, **101**(D4), 9017–9021.
- Naja, M., and H. Akimoto (2004), Contribution of regional pollution and long-range transport to the Asia-Pacific region: Analysis of long-term ozonesonde data over Japan, *J. Geophys. Res.*, **109**, D21306, doi:10.1029/2004JD004687.
- Newchurch, M. J., E.-S. Yang, D. M. Cunnold, G. C. Reinsel, J. M. Zawodny, and J. M. Russell III (2003), Evidence for slowdown in stratospheric ozone loss: First stage of ozone recovery, *J. Geophys. Res.*, **108**(D16), 4507, doi:10.1029/2003JD003471.
- Oltmans, S. J., II, et al. (1998), Trends of ozone in the troposphere, *Geophys. Res. Lett.*, **25**(2), 139–142.
- Randel, W. J., and J. B. Cobb (1994), Coherent variations of monthly mean total ozone and lower stratosphere temperature, *J. Geophys. Res.*, **99**(D3), 5433–5447.
- Reinsel, G. C., E. Weatherhead, G. C. Tiao, A. J. Miller, R. M. Nagatani, D. J. Wuebbles, and L. E. Flynn (2002), On detection of turnaround and recovery in trend for ozone, *J. Geophys. Res.*, **107**(D10), 4078, doi:10.1029/2001JD000500.
- Solomon, S., R. W. Portmann, R. R. Garcia, L. W. Thomason, L. R. Poole, and M. P. McCormick (1996), The role of aerosol variations in anthropogenic ozone depletion at northern midlatitudes, *J. Geophys. Res.*, **101**(D3), 6713–6727.
- Stolarski, R. S., P. Bloomfield, R. D. McPeters, and J. R. Herman (1991), Total ozone trends deduced from Nimbus 7 TOMS data, *Geophys. Res. Lett.*, **18**(6), 1015–1018.
- Stratospheric Processes and Their Role in Climate (SPARC) (1998), SPARC/IOC/GAW assessment of trends in the vertical distribution of ozone, edited by N. Harris, R. Hudson, and C. Phillips, *SPARC Rep. 1*, 289 pp., Verrieres le Buisson, France.
- Tarasick, D. W., D. I. Wardle, J. B. Kerr, J. J. Bellefleur, and J. Davies (1995), Tropospheric ozone trends over Canada: 1980–1993, *Geophys. Res. Lett.*, **22**(4), 409–412.
- Thompson, A. M., and R. D. Hudson (1999), Tropical tropospheric ozone (TTO) maps from Nimbus 7 and Earth Probe TOMS by the modified-residual method: Evaluation with sondes, ENSO signals, and trends from Atlantic regional time series, *J. Geophys. Res.*, **104**(D21), 26,961–26,975.
- Thompson, A. M., et al. (2003), Southern Hemisphere Additional Ozonesondes (SHADOZ) 1998–2000 tropical ozone climatology: 1. Comparison with Total Ozone Mapping Spectrometer (TOMS) and ground-based measurements, *J. Geophys. Res.*, **108**(D2), 8238, doi:10.1029/2001JD000967.
- Wang, H. J., D. M. Cunnold, L. W. Thomason, J. M. Zawodny, and G. E. Bodeker (2002), Assessment of SAGE version 6.1 ozone data quality, *J. Geophys. Res.*, **107**(D23), 4691, doi:10.1029/2002JD002418.
- Weatherhead, E. C., et al. (2000), Detecting the recovery of total column ozone, *J. Geophys. Res.*, **105**(D17), 22,201–22,210.
- World Meteorological Organization (WMO) (1990), Reports of the International Ozone Trend Panel: 1988, *Global Ozone Res. Monit. Proj. Rep. 18*, Geneva, Switzerland.
- World Meteorological Organization (WMO) (2003), Scientific assessment of ozone depletion: 2002, *Global Ozone Res. Monit. Proj. Rep. 47*, Geneva, Switzerland.
- Ziemke, J. R., and S. Chandra (1999), Seasonal and interannual variabilities in tropical tropospheric ozone, *J. Geophys. Res.*, **104**(D17), 21,425–21,442.
- Ziemke, J. R., and S. Chandra (2003a), La Niña and El Niño–induced variabilities of ozone in the tropical lower atmosphere during 1970–2001, *Geophys. Res. Lett.*, **30**(3), 1142, doi:10.1029/2002GL016387.
- Ziemke, J. R., and S. Chandra (2003b), A Madden-Julian Oscillation in tropospheric ozone, *Geophys. Res. Lett.*, **30**(23), 2182, doi:10.1029/2003GL018523.
- Ziemke, J. R., and J. L. Stanford (1994), Quasi-biennial oscillation and tropical waves in total ozone, *J. Geophys. Res.*, **99**(D11), 23,041–23,056.
- Ziemke, J. R., S. Chandra, R. D. McPeters, and P. A. Newman (1997), Dynamical proxies of column ozone with applications to global trend models, *J. Geophys. Res.*, **102**(D5), 6117–6129.
- Ziemke, J. R., S. Chandra, and P. K. Bhartia (1998), Two new methods for deriving tropospheric column ozone from TOMS measurements: Assimilated UARS MLS/HALOE and convective-cloud differential techniques, *J. Geophys. Res.*, **103**(D17), 22,115–22,127.
- Ziemke, J. R., S. Chandra, and P. K. Bhartia (2001), “Cloud slicing”: A new technique to derive upper tropospheric ozone from satellite measurements, *J. Geophys. Res.*, **106**(D9), 9853–9867.
- Ziemke, J. R., S. Chandra, and P. K. Bhartia (2003), Upper tropospheric ozone derived from the cloud slicing technique: Implications for large-scale convection, *J. Geophys. Res.*, **108**(D13), 4390, doi:10.1029/2002JD002919.

P. K. Bhartia, S. Chandra, and J. R. Ziemke, NASA Goddard Space Flight Center, Code 916, Greenbelt, MD 20771, USA. (ziemke@jwoc.y.gsfc.nasa.gov)